

1 **Title:** Drone data reveal heterogeneity in tundra greenness and phenology not captured by
2 satellites

3

4 **Authors:** Jakob J. Assmann¹, Isla H. Myers-Smith², Jeffrey T. Kerby³, Andrew M. Cunliffe⁴,
5 Gergana N. Daskalova²

6

7 **Affiliations:** ¹ Department of Biology, Aarhus University, DK

8 ² School of GeoSciences, University of Edinburgh, UK

9 ³ Aarhus Institute of Advanced Studies, Aarhus University, DK

10 ⁴ Department of Geography, University of Exeter, UK

11

12 **ORCID:** Jakob J. Assmann: 0000-0002-3492-8419

13 Isla H. Myers-Smith: 0000-0002-8417-6112

14 Jeffrey T. Kerby: 0000-0002-2739-9096

15 Andrew M. Cunliffe: 0000-0002-8346-4278

16 Gergana Daskalova: 0000-0002-5674-5322

17

18 **Abstract:**

19

20 Data across scales are required to monitor ecosystem responses to rapid warming in the
21 Arctic and to interpret tundra greening trends. Here, we tested the correspondence among
22 satellite- and drone-derived seasonal change in tundra greenness to identify optimal spatial
23 scales for vegetation monitoring on Qikiqtaruk - Herschel Island in the Yukon Territory,
24 Canada. We combined time-series of the Normalised Difference Vegetation Index (NDVI)
25 from multispectral drone imagery and satellite data (Sentinel-2, Landsat 8 and MODIS) with
26 ground-based observations for two growing seasons (2016 and 2017). We found high
27 cross-season correspondence in plot mean greenness (drone-satellite Spearman's ρ
28 0.67-0.87) and pixel-by-pixel greenness (drone-satellite R^2 0.58-0.69) for eight one-hectare
29 plots, with drones capturing lower NDVI values relative to the satellites. We identified a
30 plateau in the spatial variation of tundra greenness at distances of around half a metre in the
31 plots, suggesting that these grain sizes are optimal for monitoring such variation in the two
32 most common vegetation types on the island. We further observed a notable loss of
33 seasonal variation in the spatial heterogeneity of landscape greenness (46.2 - 63.9%) when
34 aggregating from ultra-fine-grain drone pixels (approx. 0.05 m) to the size of medium-grain
35 satellite pixels (10 – 30 m). Finally, seasonal changes in drone-derived greenness were
36 highly correlated with measurements of leaf-growth in the ground-validation plots (mean
37 Spearman's ρ 0.70). These findings indicate that multispectral drone measurements can
38 capture temporal plant growth dynamics across tundra landscapes. Overall, our results
39 demonstrate that novel technologies such as drone platforms and compact multispectral
40 sensors allow us to study ecological systems at previously inaccessible scales and fill gaps
41 in our understanding of tundra ecosystem processes. Capturing fine-scale variation across
42 tundra landscapes will improve predictions of the ecological impacts and climate feedbacks
43 of environmental change in the Arctic.

44

45 **Keywords:** Arctic tundra, vegetation monitoring, landscape phenology, satellite, drones,
46 UAV and RPAS, NDVI, scale

47 Introduction

48

49 Identifying the scales at which ecological processes operate is a fundamental, yet often
50 neglected element of ecological research (1–3). Cross-scale ecological information can
51 inform our understanding of the causes and consequences of global change (2). In tundra
52 ecosystems, vegetation responses triggered by rapid Arctic warming could influence
53 ecosystem functions through altered carbon and nutrient cycles with potential feedbacks to
54 the global climate system (4–8). Yet, challenging logistics have limited the extent of
55 field-based observations in Arctic ecosystems (9–11). The grain sizes of global-extent
56 satellite products (tens of meters to kilometres) are too coarse to capture the fine-scale
57 dynamics of tundra plants (12–14) and to link vegetation change to key ecosystem functions
58 (13). Thus, by bridging this “scale-gap”, we can transform our understanding of pan-Arctic
59 tundra vegetation change and associated global-scale climate feedbacks.

60

61 *Satellites show greening of the tundra*

62

63 Satellite observations indicate a ‘greening’ of tundra ecosystems (13,15–20) and shifts in
64 growing season phenology over recent decades (21–24). Observations of increasing tundra
65 greenness are often reported from surface-reflectance-derived Normalised Difference
66 Vegetation Index (NDVI) (16,18,25,26). Satellite-observed tundra greening has occurred
67 concurrently with ground-based observations of vegetation change in Arctic ecosystems (27)
68 including increased shrub cover (28–31) and taller community level plant height (32), as well
69 as earlier leaf emergence and flowering at some (33–36), but not all tundra sites (37–39).
70 However, mismatches between ground and satellite-based observations suggest the
71 potential for an observational scale gap (13).

72

73 *Arctic vegetation change and phenology have been linked to warming*

74

75 Satellite-observed Arctic greening trends have been linked directly to warming air
76 temperatures (19,20,40–46) and indirectly to sea-ice declines (17,47–51). Ground-based
77 observations of tundra vegetation change correspond with warming (27,32,52), but do not
78 always co-occur with satellite greening trends in the regions around the ecological
79 monitoring sites (13,53). While satellite-based phenology observations from the Arctic have
80 been mainly linked to temperature (22,54,55), *in situ* phenology in the tundra has been
81 shown to be influenced by a suite of interacting factors rarely tested in satellite-based
82 analysis of Arctic phenology. These factors include, but are not limited to: snowmelt,
83 temperature, day length, and the proximal influences of sea-ice on localised climate affect
84 (34–36,38,56,57). Thus, ecological studies indicate greater complexity of drivers than
85 analyses of satellite-derived greening trends to date.

86

87 *Inconsistencies amongst satellite platforms and heterogenous greening trends*

88

89 Greening trends and phenology measures derived from different satellite platforms do not
90 always correspond with each other (13,18). Additionally, satellite-derived greening trends
91 vary at global (18), continental (42,58–60) and regional scales (46–48,61–64). Many areas
92 of the Arctic show no trends in NDVI, with only around 20% of the Arctic spectrally greening

93 and around 1 - 4% of the Arctic spectrally browning (13,62,65,66). Recent analyses suggest
94 a slowdown of the Arctic-wide spectral greening trend over the past decade (43,67).
95 Furthermore, despite NDVI being related to the photosynthetically active biomass in the
96 tundra (14,68–70), geophysical, environmental and ecological factors, such as low solar
97 angle, atmospheric effects (including cloud and fog), snow cover, soil moisture and standing
98 water, in addition to the non-linearity of NDVI-biomass relationships, complicate the
99 interpretation of satellite-derived NDVI time-series at high latitudes (13,71). The growing
100 complexity highlighted in Arctic greening trends has led to repeated calls for ground
101 validation of satellite observations (11,18,59,60,66,72,73).

102

103 *The scale discrepancy problem in Arctic greening*

104

105 A major problem in linking satellite-derived trends of tundra spectral greenness and
106 phenology to *in situ* observations of ecological processes is the discrepancy in observational
107 scales (13,29,61,72,74). Satellite datasets with long-term records are limited by their
108 moderate- to coarse-grain sizes, ranging from 30 m (Landsat) to 250 m (MODIS) and 8 km
109 (AVHRR-GIMMS3g). *In situ* ecological monitoring in the Arctic is logistically challenging and
110 therefore restricted in extent to a limited number of sites and often metre-squared plots
111 (10,75). Only a few studies have linked on-the-ground vegetation or phenology change to
112 satellite trends in NDVI in Arctic tundra (13,14,47,48,53,76–78). However, drones equipped
113 with compact sensors now allow for the collection of ultra-fine-grain multispectral imagery at
114 landscape extents that can potentially bridge the scale-gap between satellite and
115 ground-based observations (14,79–82).

116

117 *Novel drone data to study variation in greenness*

118

119 Here, we set out to test whether drones can be used to identify the key ecological scales for
120 studying tundra greenness on Qikiqtaruk in the Canadian Arctic by bridging the scale gap
121 between satellite and *in situ* data. First, we tested whether satellite- and drone-derived
122 measures of mean landscape-scale greenness (NDVI) agree across two growing seasons
123 while controlling for the potentially confounding effects of topography and land cover.
124 Second, we identified the key spatial scales for ecological variation in landscape greenness
125 within the two most common vegetation types at our study site using variograms. Third, we
126 tested how the magnitude of seasonal variation in tundra greenness scales across grain
127 sizes from fine-resolution drone imagery to medium-grain satellite imagery. Finally, we
128 assessed whether drone-derived NDVI corresponds with on-the-ground measures of within
129 growing season change in plant growth based on methods frequently used by long-term
130 field-based monitoring networks. Thus, in our analysis we validated satellite-derived
131 landscape estimates of vegetation greenness with ultra-fine-grain drone data and described
132 spatial and temporal variation in tundra productivity at landscape extents (1-100 ha) with
133 grain sizes that were previously not accessible.

134

135 **Methods**

136

137 *Site description: Qikiqtaruk - Herschel Island*

138

139 Qikiqtaruk (69.57 N, 138.91 W) is located in the Beaufort Sea along the coastline of the
140 North Slope of the Yukon Territory, Canada. The vegetation is characteristic moist acidic
141 shrub tundra (83) found in the Western Arctic regions of North America that has experienced
142 strong spectral greening in recent decades (13). The two most common plant communities
143 on the island are the tussock sedge (“Herschel”) and Dryas-vetch (“Komakuk”) vegetation
144 types (84,85). The tussock sedge vegetation is dominated by the name-giving tussock sedge
145 *Eriophorum vaginatum* L. with varying cover of *Salix pulchra* Cham. The top-soils of the
146 island are underlain by ice-rich permafrost and undergo frequent disturbance (85). The
147 Dryas-vetch vegetation is particularly found on ground disturbed by soil creep and is
148 characterised by the near ubiquitous presence of *Dryas integrifolia* Vahl., the willow *Salix*
149 *arctica* Phall., various grass species including *Arctagrostis latifolia*. (R.Br.) Griseb. and forb
150 species (86). The relative abundances of these species are shown in (Figure S1). Though
151 the two vegetation types are specific to the region, these plant communities would group
152 with tundra types S1, W2 and G3/4 of the Circumpolar Arctic Vegetation Map (87).

153

154 We established four study areas on the east end of the island, each with two co-located
155 one-hectare plots in the two key vegetation cover types (Figure 1, Table S1). We selected
156 plots with homogenous terrain and land cover to represent the two key vegetation types and
157 to control for the potentially confounding effects of terrain and cover heterogeneity. The
158 island harbours small herds of caribou (100s of individuals) and muskox (3 - 35 individuals in
159 recent years) of fluctuating size, as well as cyclic populations of voles and lemmings (88).
160 We estimate the overall impact of herbivory on the vegetation in our study plots to be low
161 particularly in 2016 and 2017 when there were few muskox on the island.

162

163 *Multispectral drone time-series*

164

165 We analysed a total of 62 drone surveys from 21 dates; see Table S2 for a breakdown by
166 one-hectare monitoring plots. We collected multispectral drone imagery using Parrot
167 Sequoia (Paris, France) compact multispectral sensors mounted on multi-rotor drone
168 platforms in June to August in 2016 and 2017. We used three different drone platforms: a
169 Tarot 680 Pro hexacopter with camera sensor stabilisation in 2016, and a 3DR Iris+ and a
170 DJI Phantom 4 Pro without sensor stabilisation in 2017. Surveys were flown using parallel
171 flight lines (a lawn-mower flight pattern) at an altitude of ca. 50 m, giving ground-sampling
172 distances of 0.04 m to 0.06 m. Images were acquired with 75% front- and side-lap as close
173 as possible to solar noon (mean absolute difference to solar noon 2.16 h, maximum 6-7 h).
174 See Table S2 and the methods section of the Supplementary Materials for further details on
175 the drone surveys, including additional information on radiometric calibration, as well as
176 temporal and spatial coverage.

177

178 We processed the Sequoia imagery using Pix4D Mapper v4.0.21 (Lausanne, Switzerland)
179 with the *agMultispectral* template and the ‘merge map tiles’ option set to true to generate
180 co-registered single-band surface reflectance maps. Radiometric calibration was carried out
181 in Pix4D Mapper using pre- or post-flight imagery of calibrated reflectance panels; in 2016
182 we used a MicaSense (Seattle, USA) panel and in 2017 a SphereOptics (Herrsching,
183 Germany) Zenith Lite panel. We measured panel reflectance pre- and post- season and
184 used the mean values for radiometric calibration. We also calibrated for sensor properties

185 and sun irradiance measured by the incident light sensor. We used four to six ground control
186 points per survey precisely geolocated with a GNSS system to spatially constrain the
187 reconstructions in Pix4D Mapper with an estimated accuracy of 1-2 pixels between bands
188 and 2-6 pixels between surveys (81). We calculated the Sequoia NDVI as the normalised
189 difference between the near-infrared (770 nm – 810 nm) and red (640 nm – 680 nm) bands
190 of sensor.

191

192 *Satellite time-series*

193

194 Satellite time-series were obtained from three different satellite sensors: 1) the Moderate
195 Resolution Imaging Spectroradiometer (MODIS) on the USGS Terra satellite, 2) the
196 Multispectral Instrument (MSI) on Sentinel-2 A & B and 3) the Operational Land Imager (OLI)
197 on Landsat 8.

198

199 We obtained MODIS NDVI values for the time period from the 1st May to the 30th of
200 September in 2016 and 2017 for all 250 m MODIS pixels that contained the survey plots.
201 NDVI values were retrieved from the 16-day MOD13Q1 v6 Terra product (89) using the
202 Google Earth Engine (90). We discarded all values with a 'Summary QA' score of -1 (no
203 data) or 3 (cloudy). Table S3 lists the resulting MODIS-pixel-date pairs. The MODIS NDVI is
204 calculated as the normalised difference between bands 1 (841 nm – 876 nm) and band 2
205 (620 nm – 670 nm).

206

207 For the Sentinel-2 time-series, we gathered all Sentinel-2 MSI L1C scenes containing the tile
208 covering Qikiqtaruk (T07WET) that were available on the Copernicus Open Access Hub
209 (<https://scihub.copernicus.eu/>) for the same time period as the MODIS pixels. We processed
210 all scenes to L2A using Sen2Cor 2.4.0 (91), retained all bands with 10 m resolution (2-4 &
211 8), applied the cloud mask and generated a true-colour image. We inspected all scenes
212 visually and discarded all imagery with cloud contamination over the study area (78% of
213 scenes for 2016 and 74% of scenes for 2017). The resulting set contained nine cloud-free
214 Sentinel-2 L2A scenes of the study area from 2016 and fifteen scenes from 2017 (Table S4).
215 Finally, the Sentinel NDVI was calculated as the normalised difference between band 8
216 (784.5 nm - 899.5 nm) and band 4 (650 nm - 680 nm).

217

218 Landsat 8 OLI Level-2 (surface reflectance) time-series were obtained using the USGS
219 EarthExplorer website (<https://earthexplorer.usgs.gov/>) by querying the search engine for all
220 scenes that covered the study site during the same time-period as the MODIS pixels (n =
221 94). The automatically generated cloud masks were of insufficient quality, so we manually
222 inspected all scenes and retained only the scenes cloud-free over the study site (n = 7 for
223 2016, n = 8 for 2017, Table S5). The Landsat 8 NDVI was then calculated as the normalised
224 difference between band 5 (845 - 885 nm) and band 4 (630 - 680 nm). The study plots were
225 not designed with a Landsat 8 analysis in mind and did not naturally coincide with the
226 Landsat grid. We therefore calculated subsequent one-hectare plot NDVI averages as a
227 weighted mean, where each pixel was weighted by the proportion of the plot area covered
228 by the pixel.

229

230 *Ground-based plant phenology measurements*

231

232 We carried out ground-based phenology monitoring in eight 2 m x 2 m plots (Table S6), one
233 adjacent to each one-hectare plot (mean distance = 23 m, max distance = 52 m). We placed
234 the ground-based monitoring plots adjacent to the drone-based survey plots to minimise the
235 effects of ecological disturbance and trampling in the drone-based survey plots caused by
236 the repeat visits necessary for the ground-based monitoring. Within these plots we
237 monitored six individual plants from the most common species: *E. vaginatum*, *D. integrifolia*,
238 *S. pulchra* and *A. latifolia* in tussock sedge tundra; *D. integrifolia*, *S. arctica* and *A. latifolia* in
239 Dryas-vetch tundra. We measured the length of the longest leaf on each individual on the
240 survey date to the nearest millimetre. This approach is widely used in field-based phenology
241 monitoring protocols (92), and will allow for NDVI to be directly related to phenological
242 changes in plant traits. We conducted ground-based surveys in tandem with the
243 drone-based surveys where logistical possible, resulting in a dataset of 52 drone and ground
244 survey pairs spread over 20 different dates. The majority of ground-based phenology
245 surveys were carried out on the same day as the drone surveys (mean difference = 0.3
246 days, maximum difference = 3 days, Table S7).

247

248 *Cross-sensor correspondence*

249

250 To test cross-sensor correspondence, we first had to scale all datasets to a shared spatial
251 grain and time-window. To achieve this, we first plotted the spatial mean NDVI for all
252 one-hectare plots, time-points and available sensors (MODIS = single pixel, Landsat 8 =
253 weighted mean) across both growing seasons (2016 and 2017). We then divided the two
254 growing seasons into 22 consecutive seven-day blocks starting on the 1st of May each year.
255 Next, we calculated the temporal mean of the spatial mean NDVI for each seven-day block
256 for all plot and sensor combinations where data was available. We then identified all
257 matching seven-day block and study plot combinations for each drone-satellite and
258 satellite-satellite combination. We then tested cross-sensor correspondence by calculating
259 Spearman's rank correlation and mean sensor-to-sensor difference in the plot means across
260 the whole data set.

261

262 Additionally, we matched all drone and Sentinel-2 scenes, as well as all drone and Landsat 8
263 scenes that were less than two days apart. We resampled the red and near-infrared drone
264 bands to the relevant Sentinel-2 / Landsat 8 grids and calculated the NDVI. We restricted the
265 analysis to Landsat 8 pixels fully contained within the study plots and reprojected the drone
266 data from UTM 7N to UTM 8N using a bilinear reprojection where the Landsat 8 scenes
267 were provided in this projection. Finally, we tested the predictive relationship between the
268 resampled drone and satellite NDVI pixel-pairs for a random subsample of Sentinel pixels
269 (10% of total, n = 700) and all available Landsat 8 pixels (n = 198) with Bayesian linear
270 models (Table S8 and S9 for Sentinel-2, S10 and S11 for Landsat 8) using the MCMCglmm
271 v.2.29 package (93).

272

273 We used the 'resample' function of the R raster package v. 3.0-12 (94) for resampling from
274 finer to coarser resolutions. The function first aggregates the smaller grid to the largest clean
275 divisor of the larger grid using the mean and then, if required, resamples to the larger grid
276 using bilinear interpolation. We also tested an alternative resampling approach by first

277 resampling to a common resolution and grid of 0.5 m and then aggregating by mean, but
278 found no qualitative differences in our results (Figure S2). Further details about software and
279 package versions used for raster manipulations and visualisations can be found in the
280 Supplementary Materials.

281

282

283 *Spatial autocorrelation*

284

285 To assess the spatial autocorrelation of variation in tundra greenness within the eight plots,
286 we sampled variograms and fitted variogram models using the gstat v. 2.0-5 package
287 (95,96). First, we pre-thinned the acquired drone-data by randomly sampling 5% of the ca. 4
288 million pixels of each orthomosaic. We then sampled variograms for all plots at the peak of
289 the 2017 season (26 and 28 July) and fitted variogram models, letting the gstat algorithm
290 select the best fit amongst spherical, exponential and Matern models. The only exception
291 was Area 3 for which the closest available complete set of flights was on the 18th July 2017.
292 To test conformity of the variograms across the season, we repeated the analysis for the
293 surveys from the 26 June and 9 August 2017 for Area 1 and 2. No change in the variogram
294 patterns were observed across the 2017 season and we therefore assume that our analysis
295 is representative for the 2016 season also. All variograms were sampled with a bin width of
296 0.15 m from 0 to 15 m and a bin width of 3 m from 0 to 45 m.

297

298 *Grain size and phenology*

299

300 We tested the influence of grain-size on observations of tundra greenness phenology by
301 fitting simplified growing season curves to the raster stacks for each plot and season. We
302 first resampled the drone bands for all time-points to grids with grain sizes of 0.5, 1, 5, 10, 20
303 and 33.33 m. We then calculated the NDVI and fitted simple quadratic models to each pixel
304 in the growing season stacks ($y = ax^2 + bx + c$, where x is the day of year and y the pixel
305 NDVI, a the quadratic coefficient, b the linear coefficient and c the constant term). We found
306 a strong negative correlation between the quadratic and linear coefficients of the models
307 (Figure S6), we selected only the quadratic coefficient for further analysis. Further details on
308 model choice and analysis can be found in the method section of the Supplementary
309 Materials.

310

311 *Ground validation*

312

313 To test the correspondence between our ground-based phenology measurements and the
314 drone observations, we derived time-series of the plot mean standardised longest leaf length
315 for all species (using a z-score – centred data with a standard deviation of 1) and the
316 drone-greenness for each 2 m x 2 m ground-based monitoring plot. See supplementary
317 methods for details on how the leaf measurements were standardised. The drone-based plot
318 mean NDVI values were then matched with the plot mean standardised longest leaf length
319 values from the closest ground-based survey date (Table S7). We then calculated the
320 Spearman's rank correlation between mean NDVI and mean longest standardised leaf
321 length for each plot and season. We replicated the analysis using Sentinel-2 data where
322 available (see Supplementary Materials). Finally, we also conducted a by-species version of

323 the analysis using the by-species mean of the absolute longest leaf measurements for each
324 2 m x 2 m plot rather than the mean based on the standardised longest leaf measurements.

325

326 **Results**

327

328 *Landscape greenness corresponded among sensors*

329

330 Landscape greenness corresponded well among drone, Sentinel-2, Landsat 8 and MODIS
331 across both the 2016 and 2017 growing seasons. Growing season curves of the plot mean
332 NDVI were similar (Figure 1) and the seven-day block plot mean NDVI values were highly
333 correlated across sensors (Spearman's $\rho > 0.59-0.98$, Table S12). However, we observed a
334 positive offset between drone and satellite plot-mean NDVI for the seven-day block means
335 between 0.027 (Landsat 8) and 0.073 (Sentinel-2B) absolute NDVI that was consistent
336 across satellite platforms (Table S13). The Landsat 8 offset of 0.027 fell within the range of
337 the estimated error associated (± 0.03) with the drone-derived plot mean NDVI for the study
338 plots determined previously with the same survey method (81).

339

340 Resampled drone pixels (10 m and 30 m) and the corresponding spatially co-located
341 Sentinel-2 and Landsat 8 pixels were highly correlated (marginal $R^2 = 0.69$ and marginal R^2
342 $= 0.58$ respectively, see Figure 2 and Table S8 and S10). We found that vegetation type, the
343 time-difference between satellite scene and drone data acquisition, and the specific Sentinel
344 platform (Sentinel-2A / Sentinel-2B) influenced the relationship between Sentinel-2 pixel
345 NDVI and drone-derived NDVI (marginal $R^2 = 0.87$ see Table S9). While the Sentinel
346 platform (Sentinel-2A / Sentinel-2B) had the strongest impact on the intercept and slope of
347 the linear model, vegetation type and time-difference mainly influenced the slope, with
348 time-difference having the smallest effect on slope and intercept overall (Table S9). In
349 contrast, we only detected a statistically meaningful difference in days between satellite and
350 drone scene acquisition for the Landsat 8 - drone pixel model (marginal $R^2 = 0.70$);
351 vegetation type did not have a statistically meaningful influence on this relationship (Table
352 S11).

353

354 *Spatial variation in landscape greenness peaked at approx. 0.5 m*

355

356 Spatial variability in the NDVI values associated with distance peaked at ranges below 0.5
357 meter (mean range 0.44 m) during the peak-season of 2017 (26-28 July), and little additional
358 autocorrelation structure in the NDVI was found between pixel pairs for distances of up to 45
359 m (Figure 3). This pattern was consistent across vegetation types in seven out of our eight
360 plots (Figure 3, S3 and S4). The only exception is the Dryas-vetch plot in Area 3, which
361 showed the same patterns for distance below 10 m, but thereafter spatial variation steadily
362 increased (Figure S4). Peak variability (sill) in NDVI decreased as the growing season
363 progressed (Figure S5), and varied with vegetation type (Figure 3, S3, and S4). Unexplained
364 variability (nugget) was consistently low across all Areas (Figure 3, S3, and S4).

365

366

367 *Seasonal-variation was lost when aggregating to medium grain sizes*

368

369 We observed a notable loss in the amount of seasonal variation in tundra greenness when
370 aggregating grain size from ultra-fine-grain drone to medium-grain satellite data. The loss
371 was particularly pronounced at grain-sizes above 10 m – the grain size of Sentinel-2 MSI
372 pixels (46.2 - 63.9%) (Figure 4). The variation in the quadratic coefficient of the simple
373 growing season curves (Figure 4b and S6) decayed logarithmically with grain size (Figure
374 4a), while no change occurred in the mean tendency of the coefficient (Figure S7). The
375 quadratic and linear coefficients of the growing season curves were strongly correlated
376 (Spearman's $\rho = -0.999$), thus the same pattern holds true for the linear component of the
377 curve fit (Figure S6).

378

379 *Drone-derived spectral greenness correlated well with leaf measurements*

380

381 Drone-derived spectral greenness correlated well (mean $\rho = 0.70$) with ground-based
382 measurements of cross-season phenology for graminoids and deciduous plants (Figure 5).
383 The Spearman's correlation coefficient of the plot mean standardised leaf length and the
384 mean drone-derived NDVI values in the ground-based phenology plots (mean $\rho = 0.70$,
385 Table S14 and Figure 5) matched the by-species analysis based on absolute leaf lengths
386 (mean $\rho = 0.68$, Table S15 and Figure S9). The graminoids and deciduous shrub species
387 followed this mean tendency well across all time-series, while the partially-evergreen *D.*
388 *integrifolia* showed mixed responses between plots and years (mean $\rho = 0.22$, Figure S9).
389 The drone-based greenness time-series of the 2 m x 2 m ground-phenology plots highlight
390 fine-scale differences in phenology such as the continuous greening of tussocks that was
391 visible at the tussock sedge tundra plot in Area 2 (Figure 5c). Sentinel-2 greenness showed
392 slightly weaker correlations (mean $\rho = 0.58$, Figure S10) with the plot mean standardised
393 leaf length, but no combined Sentinel-2 and ground-based phenology time-series of
394 sufficient length were available for 2016 and peak-season observations in 2017 were limited.

395

396 **Discussion**

397

398 Our analysis of cross-scale time-series of landscape greenness on Qikiqtaruk highlights four
399 main findings: 1) Measures of mean tendency in landscape greenness were consistent
400 across sensors, but drone-derived NDVI values were lower than those from Sentinel-2,
401 Landsat 8 and MODIS products (Figures 1 and 2). 2) The majority of variation in landscape
402 greenness was contained at scales of around half-a-metre, and is thus not captured by
403 medium-grain satellites such as Sentinel-2 (Figure 3). 3) When aggregating growing season
404 curves from ultra-fine-grain drone to medium-grain satellite pixel sizes, a notable amount
405 (46.2 - 63.9%) of variation in greenness phenology was lost (Figure 4). 4) Drone-based
406 measures of landscape greenness correlated well with ground-based measurements of leaf
407 length (Figure 5). Taken together, our results highlight that drone platforms and compact
408 multispectral sensors can capture key ecological processes such as vegetation phenology
409 and bridge the existing scale gap between satellite and ground-based monitoring in tundra
410 ecosystems.

411

412 The correspondence between drone and satellite-derived NDVI has yet to be
413 comprehensively tested across Arctic sites (13,14). Siewert and Olofson (14) also
414 demonstrate cross-sensor agreement between drone- and satellite-derived NDVI from Arctic

415 Sweden. While similar or higher levels of cross-sensor agreement have been observed in
416 other natural and agricultural systems (14,97,98), some non-Arctic studies showed mixed or
417 poor agreement (99–101). Continued efforts in replicating these studies at different study
418 sites and systems is much needed to comprehensively evaluate cross-sensor
419 correspondence in Arctic tundra systems and beyond.

420

421 We observed a small but consistent offset between drone- and satellite-derived NDVI that
422 warrants further investigation. A similar offset has been detected in rice fields in Italy (100)
423 and with spectroradiometer readings in ecologically similar tundra in Alaska (77), but see
424 Siewert and Olofson (14) for a lack of offset in the more heterogeneous tundra of Arctic
425 Sweden. Both technical and ecological factors could explain the offset. We were not able to
426 conduct spectroradiometer readings coinciding with our drone surveys for on-the-ground
427 comparisons. Technical reasons for the observed offset may include: atmospheric effects,
428 differences in viewing geometries, sensor properties (e.g. band widths) and signal
429 processing (e.g. radiometric calibration) between drones and satellites, but also among
430 different drone studies. Ecologically, the variation in land cover (especially the
431 presence/absence of non-vegetative surfaces) or topography within a landscape may
432 influence correspondence between vegetation greenness across scales due to
433 non-linearities in how aggregating different patch sizes and cover types influence measures
434 of NDVI (12,102). The high homogeneity of the survey plots on Qikiqtaruk likely contributes
435 to the strong correlation between drone- and satellite-derived NDVI that we have observed.
436 Yet, in our drone data fine-grain patterns of higher and lower NDVI within the landscape
437 including bare-ground patches and areas of more productive vegetation in wetter parts of the
438 landscape were evident (Figures 1-3). Heterogeneity in land cover and landscape-level
439 variation in NDVI at different spatial scales from vegetation patterning to tundra patterns in
440 topographically variable terrain could be differentially influencing correspondence in NDVI in
441 drone and satellite data across scales. Further research is needed to evaluate cross-sensor
442 and cross-scale correspondence in NDVI and other vegetation indices across Arctic tundra
443 systems.

444

445 We found that a plateau of spatial variation in tundra greenness occurred around 0.5 m,
446 approximately the same width as biological and environmental patterning at this site. The *E.*
447 *vaginatum* sedges that dominate the tussock sedge vegetation type typically have diameters
448 of ~ 0.1 - 0.5 m (Figure 3b) (103). The tussock sedge vegetation type is underlain by
449 ice-wedge polygons that when thawed create bands of wetter or drier plant communities with
450 widths of ~ 0.5 m – 3.0 m (104). Dryas-vetch vegetation is often found on gentle sloping
451 uplands where active layer disturbances such as cryoturbation and solifluction create
452 characteristic bare-ground patches perpendicular to the slope (85) with dimensions of ~ 0.3
453 m – 0.5 m width and ~ 0.3 – 1.0 m length (Figure 3b). We expect that spatial variation would
454 increase with distances beyond the one-hectare extents of our plots as more topographic
455 diverse terrain is encountered and vegetation type transitions are reached. Topography is a
456 key proxy for many processes that structure heterogeneity in tundra vegetation (105–107)
457 and the plots were selected for little topographic variation to allow us to isolate specific
458 effects of land cover on scaling of greenness patterns from topography. The plot with the
459 highest elevational range (Area 3 - Dryas-vetch tundra: 8.7 m) showed a small but steady
460 increase in spatial variation in distance classes above 10 m (Figure S4). Our findings

461 illustrate that on Qikiqtaruk, grain sizes of 0.5 m or less are required to capture key spatial
462 variation in vegetation greenness.

463

464 In our study, ecological information was lost when upscaling from ultra-fine-grain (~ 0.05 m)
465 drone to moderate grain (~ 10 – 30m) satellite resolutions. Even the most recent generation
466 of freely-available multispectral satellite products can be limited in their ability to capture
467 fine-grain ecological processes of tundra vegetation change (13). Information transfer during
468 upscaling leads to the loss of more information in tundra ecosystems compared to other
469 biomes (14,108) as land cover and vegetation structure are fragmented at finer scales (109).
470 However, exactly how spatial aggregation influences the loss in observed ecological
471 variability across the diversity of Arctic landscapes remains poorly quantified (11). Yet, this
472 variability is critical to understanding climate-driven changes in vegetation phenology
473 (35,36,88), plant-pollinator interactions (110), and trophic interactions (111). With fine-grain
474 observations, we were able to detect a subtle decrease in the magnitude of the spatial
475 variability in landscape-level phenology as the growing season progressed (Figure S5), while
476 aggregation to moderate satellite grains obscured both the magnitude and timing of
477 phenological heterogeneity (Figure 4). Thus, time-series of fine-grain remotely-sensed
478 observations will be critical for answering key research questions about tundra ecosystem
479 functioning in a warming Arctic (112).

480

481 Our results indicate that drone-based greenness time-series captured variation in plot-level
482 leaf-growth of deciduous tundra plant species. We demonstrate how drones can be used to
483 measure variation in tundra plant phenology of metre-scale patches at landscape extents.
484 Drones have been successfully used to monitor phenology of individual plants (trees) in
485 temperate forest ecosystems (113–115), and our study indicates that individual plant-level
486 phenology monitoring of sub-decimeter variability from drones could also be carried out in
487 tundra ecosystems. Future studies that quantify plant growth or phenology events such as
488 leaf emergence and flowering across the landscape could provide key information on
489 resource availability for plant-consumer interactions (110,111). Our findings also highlight
490 known limitations of NDVI to track phenology in evergreens or other non-deciduous taxa (*D.*
491 *integrifolia*, Figure S9), suggesting that tests of alternative vegetation index - plant growth
492 relationships (115) are needed to capture within-growing-season variation in plant metabolic
493 activity of tundra evergreen and moss species. Combining drone-based time-series with
494 observations from phenocams, satellite and ground-based study plots has the potential to
495 revolutionise our understanding of landscape-scale phenology (13) by moving beyond the
496 previously small samples of individuals monitored in the Arctic tundra (36,37,39,116).

497

498 The collection of multispectral drone time-series in Arctic ecosystems has limitations and
499 challenges. Recent studies have discussed challenges with radiometric consistency and
500 repeatability when using compact multispectral drone sensors (81,117,118). Due to logistical
501 constraints, we were not able to always conduct surveys under optimal conditions due to sun
502 angle or cloud cover nor as frequently as planned due to wind or precipitation (Table S2),
503 which likely introduced bias and/or noise into our drone data (e.g., Figure 4b). Access
504 limitations meant that we could not capture spring and autumn on Qikiqtaruk. As an
505 early-generation multispectral drone sensor, the Parrot Sequoia was tailored for deriving the
506 NDVI, which despite being the legacy workhorse of tundra remote-sensing has limitations

507 (11,13). In particular, NDVI can be confounded by moisture and surface water (11,73,119),
508 complicating interpretation in wet tundra and particularly in fine-grain size data. However, the
509 rapid technological development of drones and sensors, as well as further consolidation and
510 standardisation of methods (120), will allow for pan-Arctic syntheses of fine-grain data to
511 resolve the uncertainty and complexity of Arctic greening patterns trends (13,14,81) (see
512 also the High Latitude Drone Ecology Network - <https://arcticdrones.org/>).

513

514 Our study demonstrates that drones can fill the scale-gap between satellite and field studies
515 in the observation of terrestrial Arctic vegetation change. Rather than investigating and
516 explaining patterns at scales pre-defined by satellite datasets or field-based networks,
517 researchers can use drones to identify scale-domains that are most closely associated with
518 ecological processes of interest. Field ecologists can now use scaling theory provided by the
519 remote sensing community (74,121–124) at scales and temporal intervals that will allow for
520 hypothesis testing about what mechanisms are driving landscape-level ecological change.
521 Drone imagery will also allow the remote sensing community to track the effects of sub-pixel
522 heterogeneity on satellite products down to the grain of individual plants and communities
523 (14) that have been long studied by field-based monitoring networks, like the International
524 Tundra Experiment (75). Only by improving our understanding of how ecologically important
525 information is captured across grain sizes can we reduce uncertainties in the medium- and
526 coarse-grain satellite observation that feed into Earth system models and shape their
527 predictions (4,8). Fine-scale remote sensing from drones and aircraft provides key tools for
528 disentangling the drivers behind the greening of the Arctic (14,79,112).

529

530 **Conclusions**

531

532 Novel remote-sensing technologies such as drones now allow us to study ecological
533 variation in landscapes continuously across scales. Fine-grain ecological observation is of
534 particular importance where variation in plant growth happens at very small spatial scales
535 such as in tundra ecosystems (13,71). Our finding of a peak in spatial variation found at
536 distances of ~0.5 m in the plots on Qikiqtaruk shows the grain size at which phenological
537 information within the plant communities is best captured at this site. We demonstrate that
538 key ecological information is lost when observing the tundra at even decimeter or coarser
539 scales, such as those of medium grain satellites (~ 10 – 30m). Despite the methodological
540 challenges of collecting multispectral drone imagery in remote environments (81), our
541 time-series of vegetation greenness correlated well with ground-based measurements of leaf
542 growth in the validation plots. Drones now enable cross-scale studies that fill scale gaps
543 between satellite and ground-based observations facilitating the identification of key drivers
544 of vegetation change to inform projections of climate change impacts and feedbacks in the
545 tundra biome.

546

547 **Acknowledgements**

548

549 We would like to thank the Team Shrub field crews of the 2016 and 2017 field seasons for
550 their hard work and effort invested in collecting the data presented in this research, this
551 includes Will Palmer, Santeri Lehtonen, Callum Tyler, Sandra Angers-Blondin and Haydn
552 Thomas. Furthermore, we would like to thank Tom Wade and Simon Gibson-Poole from the

553 University of Edinburgh Airborne GeoSciences Facility, as well as Chris McLellan and
554 Andrew Gray from the NERC Field Spectroscopy Facility for their support in our drone
555 endeavours. We also want to express our gratitude to Ally Phillimore, Ed Midchard and Toke
556 Høye for providing feedback on earlier versions of this manuscript.

557

558 We thank the Herschel Island - Qikiqtaruk Territorial Park Team and Yukon Government for
559 providing logistical support for our field research on Qikiqtaruk including: Richard Gordon,
560 Cameron Eckert and the park rangers Edward McLeod, Sam McLeod, Ricky Joe, Paden
561 Lennie and Shane Goosen. We thank the research group of Hugues Lantuit at the Alfred
562 Wegener Institute and the Aurora Research Institute for logistical support. Research permits
563 include Yukon Researcher and Explorer permits (16-48S&E and 17-42S&E) and Yukon
564 Parks Research permits (RE-Inu-02-16 and 17-RE-HI-02). All airborne activities were
565 licensed under the Transport Canada special flight operations certificates ATS
566 16-17-00008441 RDIMS 11956834 (2016) and ATS 16-17-00072213 RDIMS 12929481
567 (2017).

568

569 Funding for this research was provided by NERC through the ShrubTundra standard grant
570 (NE/M016323/1), a NERC E3 Doctoral Training Partnership PhD studentship for Jakob
571 Assmann (NE/L002558/1), a research grant from the National Geographic Society
572 (CP-061R-17), a Parrot Climate Innovation Grant, the Aarhus University Research
573 Foundation, and the European Union's Horizon 2020 research and innovation programme
574 under the Marie Skłodowska-Curie grant agreement (754513) for Jeffrey Kerby, a NERC
575 support case for use of the NERC Field Spectroscopy Facility (738.1115), equipment loans
576 from the University of Edinburgh Airborne GeoSciences Facility and the NERC Geophysical
577 Equipment Facility (GEF 1063 and 1069).

578

579 Finally, we would like to thank the Inuvialuit people for the opportunity to conduct research in
580 the Inuvialuit Settlement Region.

581

582 **Author Contributions**

583

584 JJA and IMS conceived the study with input from JTK and AMC. JJA carried out data
585 processing and analysis. JJA and IMS led the drone and ground-validation field work in
586 2016. AMC led the drone field surveys with input from JTK and GD led the ground-validation
587 for 2017 with input from JTK. JJA, IMS and JTK wrote the manuscript with input from AMC
588 and GD. IMS supervised and acquired funding for the research.

589

590 **Data availability**

591

592 All processed drone and Sentinel imagery is available via a data repository on Zenodo
593 (embargoed till publication of this manuscript).

594 Should the reviewers wish to access the data prior publication, a mirror of the Zenodo
595 repository can be accessed via this confidential link:

596

597

598 All code used to conduct the analysis, produce figures and as well as summary data
599 outputs and MODIS pixel values can be found on this GitHub repository (already openly
600 available):

601 https://github.com/jakobjassmann/qhi_phen_ts

602

603 **References**

604

- 605 1. Levin SA. The Problem of Pattern and Scale in Ecology: The Robert H. MacArthur
606 Award Lecture. *Ecology*. 1992 Dec 1;73(6):1943–67.
- 607 2. Anderson CB. Biodiversity monitoring, earth observations and the ecology of scale.
608 *Ecol Lett*. 2018 Oct 1;21(10):1572–85.
- 609 3. Estes L, Elsen PR, Treuer T, Ahmed L, Caylor K, Chang J, et al. The spatial and
610 temporal domains of modern ecology. *Nat Ecol Evol*. 2018 May;2(5):819.
- 611 4. Chapin FS, Sturm M, Serreze MC, McFadden JP, Key JR, Lloyd AH, et al. Role of
612 land-surface changes in arctic summer warming. *Science*. 2005 Oct
613 28;310(5748):657–60.
- 614 5. Loranty MM, Goetz SJ. Shrub expansion and climate feedbacks in Arctic tundra.
615 *Environ Res Lett*. 2012 Mar 1;7(1):011005.
- 616 6. Pearson RG, Phillips SJ, Loranty MM, Beck PSA, Damoulas T, Knight SJ, et al. Shifts
617 in Arctic vegetation and associated feedbacks under climate change. *Nat Clim Change*.
618 2013 Jul;3(7):673–7.
- 619 7. Richardson AD, Keenan TF, Migliavacca M, Ryu Y, Sonnentag O, Toomey M. Climate
620 change, phenology, and phenological control of vegetation feedbacks to the climate
621 system. *Agric For Meteorol*. 2013 Feb 15;169:156–73.
- 622 8. Ernakovich JG, Hopping KA, Berdanier AB, Simpson RT, Kachergis EJ, Steltzer H, et
623 al. Predicted responses of arctic and alpine ecosystems to altered seasonality under
624 climate change. *Glob Change Biol* [Internet]. 2014 Mar 1 [cited 2014 Apr 9]; Available
625 from: <http://onlinelibrary.wiley.com/doi/10.1111/gcb.12568/abstract>
- 626 9. Diepstraten RAE, Jessen TD, Fauvelle CMD, Musiani MM. Does climate change and
627 plant phenology research neglect the Arctic tundra? *Ecosphere*. 2018;9(9):e02362.
- 628 10. Metcalfe DB, Hermans TDG, Ahlstrand J, Becker M, Berggren M, Björk RG, et al.
629 Patchy field sampling biases understanding of climate change impacts across the
630 Arctic. *Nat Ecol Evol*. 2018 Sep;2(9):1443.
- 631 11. Beamish A, Reynolds MK, Epstein H, Frost GV, Macander MJ, Bergstedt H, et al.
632 Recent trends and remaining challenges for optical remote sensing of Arctic tundra
633 vegetation: A review and outlook. *Remote Sens Environ*. 2020 Sep 1;246:111872.
- 634 12. Stoy PC, Williams M, Disney M, Prieto-Blanco A, Huntley B, Baxter R, et al. Upscaling
635 as ecological information transfer: a simple framework with application to Arctic
636 ecosystem carbon exchange. *Landsc Ecol*. 2009 Aug 1;24(7):971–86.
- 637 13. Myers-Smith IH, Kerby JT, Phoenix GK, Bjerke JW, Epstein HE, Assmann JJ, et al.
638 Complexity revealed in the greening of the Arctic. *Nat Clim Change*. 2020
639 Feb;10(2):106–17.
- 640 14. Siewert MB, Olofsson J. Scale-dependency of Arctic ecosystem properties revealed by
641 UAV. *Environ Res Lett* [Internet]. 2020 Jul 2 [cited 2020 Jul 6]; Available from:
642 <https://iopscience.iop.org/article/10.1088/1748-9326/aba20b>
- 643 15. Myneni RB, Keeling CD, Tucker CJ, Asrar G, Nemani RR. Increased plant growth in the
644 northern high latitudes from 1981 to 1991. *Nature*. 1997 Apr;386(6626):698–702.
- 645 16. Tucker CJ, Slayback DA, Pinzon JE, Los SO, Myneni RB, Taylor MG. Higher northern
646 latitude normalized difference vegetation index and growing season trends from 1982
647 to 1999. *Int J Biometeorol*. 2001 Nov 1;45(4):184–90.
- 648 17. Bhatt US, Walker DA, Reynolds MK, Comiso JC, Epstein HE, Jia GJ, et al. Circumpolar
649 arctic tundra vegetation change is linked to sea ice decline. *Earth Interact*. 2010
650 Aug;14(8):1–20.
- 651 18. Guay KC, Beck PSA, Berner LT, Goetz SJ, Baccini A, Buermann W. Vegetation
652 productivity patterns at high northern latitudes: a multi-sensor satellite data
653 assessment. *Glob Change Biol*. 2014;20(10):3147–3158.

- 654 19. Zhu Z, Piao S, Myneni RB, Huang M, Zeng Z, Canadell JG, et al. Greening of the Earth
655 and its drivers. *Nat Clim Change*. 2016 Aug;6(8):791–5.
- 656 20. Keenan TF, Riley WJ. Greening of the land surface in the world's cold regions
657 consistent with recent warming. *Nat Clim Change*. 2018 Sep;8(9):825–8.
- 658 21. Zeng H, Jia G, Epstein H. Recent changes in phenology over the northern high
659 latitudes detected from multi-satellite data. *Environ Res Lett*. 2011;6(4):045508.
- 660 22. Zeng H, Jia G, Forbes BC. Shifts in Arctic phenology in response to climate and
661 anthropogenic factors as detected from multiple satellite time series. *Environ Res Lett*.
662 2013;8(3):035036.
- 663 23. Zhao J, Zhang H, Zhang Z, Guo X, Li X, Chen C. Spatial and Temporal Changes in
664 Vegetation Phenology at Middle and High Latitudes of the Northern Hemisphere over
665 the Past Three Decades. *Remote Sens*. 2015 Aug;7(8):10973–95.
- 666 24. Potter C, Alexander O. Changes in Vegetation Phenology and Productivity in Alaska
667 Over the Past Two Decades. *Remote Sens*. 2020 Jan;12(10):1546.
- 668 25. Tucker CJ. Red and photographic infrared linear combinations for monitoring
669 vegetation. *Remote Sens Environ*. 1979 May 1;8(2):127–50.
- 670 26. Myneni RB, Tucker CJ, Asrar G, Keeling CD. Interannual variations in satellite-sensed
671 vegetation index data from 1981 to 1991. *J Geophys Res Atmospheres*.
672 1998;103(D6):6145–60.
- 673 27. Elmendorf SC, Henry GHR, Hollister RD, Björk RG, Boulanger-Lapointe N, Cooper EJ,
674 et al. Plot-scale evidence of tundra vegetation change and links to recent summer
675 warming. *Nat Clim Change*. 2012 Apr 8;2:453–7.
- 676 28. Tape KD, Sturm M, Racine CH. The evidence for shrub expansion in Northern Alaska
677 and the Pan-Arctic. *Glob Change Biol*. 2006 Apr;12(4):686–702.
- 678 29. Myers-Smith IH, Forbes BC, Wilmsking M, Hallinger M, Lantz T, Blok D, et al. Shrub
679 expansion in tundra ecosystems: dynamics, impacts and research priorities. *Environ*
680 *Res Lett*. 2011 Dec 1;6(4):045509.
- 681 30. Tape K, Hallinger M, Welker J, Ruess R. Landscape heterogeneity of shrub expansion
682 in Arctic Alaska. *Ecosystems*. 2012;15(5):711–24.
- 683 31. García Criado M, Myers-Smith IH, Bjorkman AD, Lehmann CER, Stevens N. Woody
684 plant encroachment intensifies under climate change across tundra and savanna
685 biomes. *Glob Ecol Biogeogr*. 2020;(in press).
- 686 32. Bjorkman AD, Myers-Smith IH, Elmendorf SC, Normand S, R ger N, Beck PSA, et al.
687 Plant functional trait change across a warming tundra biome. *Nature*. 2018
688 Oct;562(7725):57–62.
- 689 33. H ye TT, Post E, Meltofte H, Schmidt NM, Forchhammer MC. Rapid advancement of
690 spring in the High Arctic. *Curr Biol*. 2007 Jun 19;17(12):R449–51.
- 691 34. Kerby JT, Post E. Advancing plant phenology and reduced herbivore production in a
692 terrestrial system associated with sea ice decline. *Nat Commun [Internet]*. 2013 Oct 1
693 [cited 2014 Oct 23];4. Available from:
694 [http://www.nature.com/ncomms/2013/131001/ncomms3514/full/ncomms3514.html?me](http://www.nature.com/ncomms/2013/131001/ncomms3514/full/ncomms3514.html?message-global=remove)
695 [ssage-global=remove](http://www.nature.com/ncomms/2013/131001/ncomms3514/full/ncomms3514.html?message-global=remove)
- 696 35. Post E, Kerby J, Pedersen C, Steltzer H. Highly individualistic rates of plant
697 phenological advance associated with arctic sea ice dynamics. *Biol Lett*. 2016 Dec
698 1;12(12):20160332.
- 699 36. Assmann JJ, Myers-Smith IH, Phillimore AB, Bjorkman AD, Ennos RE, Prev y JS, et
700 al. Local snow melt and temperature—but not regional sea ice—explain variation in
701 spring phenology in coastal Arctic tundra. *Glob Change Biol*. 2019;25(7):2258–74.
- 702 37. Oberbauer SF, Elmendorf SC, Troxler TG, Hollister RD, Rocha AV, Bret-Harte MS, et
703 al. Phenological response of tundra plants to background climate variation tested using
704 the International Tundra Experiment. *Philos Trans R Soc B Biol Sci [Internet]*. 2013 Aug

- 705 19 [cited 2013 Aug 20];368(1624). Available from:
706 <http://rstb.royalsocietypublishing.org/content/368/1624/20120481>
- 707 38. Bjorkman AD, Elmendorf SC, Beamish AL, Vellend M, Henry GHR. Contrasting effects
708 of warming and increased snowfall on Arctic tundra plant phenology over the past two
709 decades. *Glob Change Biol*. 2015 Dec 1;21(12):4651–61.
- 710 39. Prev y JS, Rixen C, R ger N, H ye TT, Bjorkman AD, Myers-Smith IH, et al. Warming
711 shortens flowering seasons of tundra plant communities. *Nat Ecol Evol*. 2019
712 Jan;3(1):45.
- 713 40. Jia GJ, Epstein HE, Walker DA. Spatial heterogeneity of tundra vegetation response to
714 recent temperature changes. *Glob Change Biol*. 2006 Jan;12(1):42–55.
- 715 41. Raynolds MK, Comiso JC, Walker DA, Verbyla D. Relationship between
716 satellite-derived land surface temperatures, arctic vegetation types, and NDVI. *Remote
717 Sens Environ*. 2008 Apr 15;112(4):1884–94.
- 718 42. Jia GJ, Epstein HE, Walker DA. Vegetation greening in the Canadian Arctic related to
719 decadal warming. *J Environ Monit*. 2009;11(12):2231.
- 720 43. Bhatt US, Walker DA, Raynolds MK, Bieniek PA, Epstein HE, Comiso JC, et al. Recent
721 declines in warming and vegetation greening trends over Pan-Arctic tundra. *Remote
722 Sens*. 2013 Aug 29;5(9):4229–54.
- 723 44. Xu L, Myneni RB, Chapin Iii FS, Callaghan TV, Pinzon JE, Tucker CJ, et al.
724 Temperature and vegetation seasonality diminishment over northern lands. *Nat Clim
725 Change* [Internet]. 2013 Mar 10 [cited 2013 Mar 12]; Available from:
726 <http://www.nature.com/nclimate/journal/vaop/ncurrent/full/nclimate1836.html>
- 727 45. Piao S, Nan H, Huntingford C, Ciais P, Friedlingstein P, Sitch S, et al. Evidence for a
728 weakening relationship between interannual temperature variability and northern
729 vegetation activity. *Nat Commun*. 2014 Oct 16;5:5018.
- 730 46. Vickers H, H gda KA, Solb  S, Karlsen SR, T mmervik H, Aanes R, et al. Changes in
731 greening in the high Arctic: insights from a 30 year AVHRR max NDVI dataset for
732 Svalbard. *Environ Res Lett*. 2016;11(10):105004.
- 733 47. Walker DA, Leibman MO, Epstein HE, Forbes BC, Bhatt US, Raynolds MK, et al.
734 Spatial and temporal patterns of greenness on the Yamal Peninsula, Russia:
735 interactions of ecological and social factors affecting the Arctic normalized difference
736 vegetation index. *Environ Res Lett*. 2009 Oct;4(4):045004.
- 737 48. Macias-Fauria M, Forbes BC, Zetterberg P, Kumpula T. Eurasian Arctic greening
738 reveals teleconnections and the potential for structurally novel ecosystems. *Nat Clim
739 Change*. 2012;2:613–618.
- 740 49. Post E. Erosion of community diversity and stability by herbivore removal under
741 warming. *Proc R Soc B Biol Sci*. 2013 Apr 22;280(1757):20122722.
- 742 50. Bhatt US, Walker DA, Walsh JE, Carmack EC, Frey KE, Meier WN, et al. Implications
743 of Arctic sea ice decline for the Earth system. *Annu Rev Environ Resour*.
744 2014;39:57–89.
- 745 51. Fauchald P, Park T, T mmervik H, Myneni R, Hausner VH. Arctic greening from
746 warming promotes declines in caribou populations. *Sci Adv*. 2017 Apr 1;3(4):e1601365.
- 747 52. Elmendorf SC, Henry GHR, Hollister RD, Fosaa AM, Gould WA, Hermanutz L, et al.
748 Experiment, monitoring, and gradient methods used to infer climate change effects on
749 plant communities yield consistent patterns. *Proc Natl Acad Sci*. 2015 Jan
750 13;112(2):448–52.
- 751 53. Pattison RR, Jorgenson JC, Raynolds MK, Welker JM. Trends in NDVI and tundra
752 community composition in the Arctic of NE Alaska between 1984 and 2009.
753 *Ecosystems*. 2015 Mar 19;18(4):707–19.
- 754 54. Piao S, Tan J, Chen A, Fu YH, Ciais P, Liu Q, et al. Leaf onset in the northern
755 hemisphere triggered by daytime temperature. *Nat Commun*. 2015 Apr 23;6:6911.

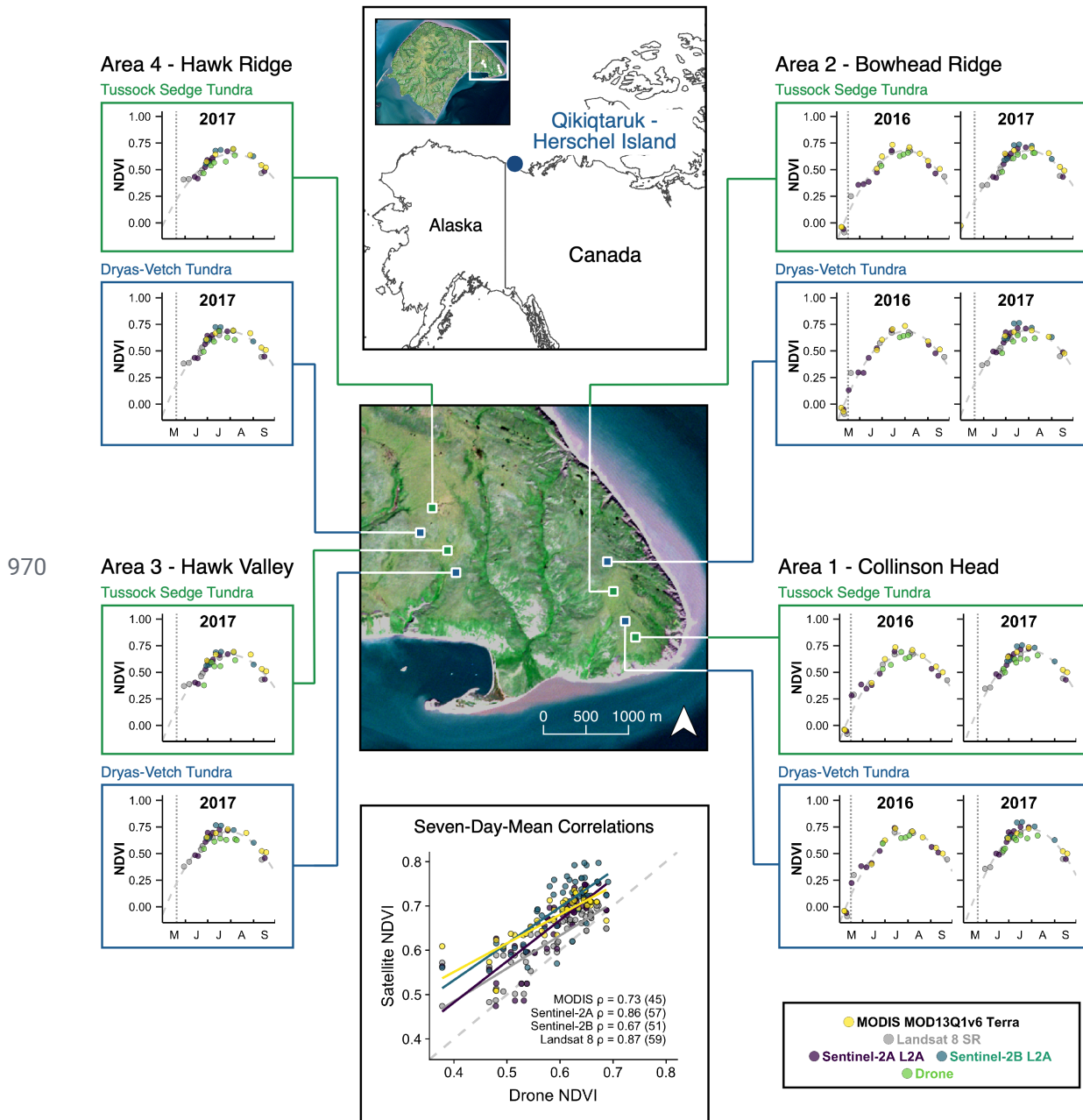
- 756 55. Liu Q, Fu YH, Zhu Z, Liu Y, Liu Z, Huang M, et al. Delayed autumn phenology in the
757 Northern Hemisphere is related to change in both climate and spring phenology. *Glob*
758 *Change Biol.* 2016 Nov 1;22(11):3702–11.
- 759 56. Semenchuk PR, Gillespie MAK, Rumpf SB, Baggesen N, Elberling B, Cooper EJ. High
760 Arctic plant phenology is determined by snowmelt patterns but duration of phenological
761 periods is fixed: an example of periodicity. *Environ Res Lett.* 2016;11(12):125006.
- 762 57. Prev y J, Vellend M, R ger N, Hollister RD, Bjorkman AD, Myers-Smith IH, et al.
763 Greater temperature sensitivity of plant phenology at colder sites: implications for
764 convergence across northern latitudes. *Glob Change Biol* [Internet]. 2017 Feb 1 [cited
765 2017 Feb 6]; Available from:
766 <http://onlinelibrary.wiley.com.ezproxy.is.ed.ac.uk/doi/10.1111/gcb.13619/abstract>
- 767 58. Jia GJ, Epstein HE, Walker DA. Greening of arctic Alaska, 1981–2001. *Geophys Res*
768 *Lett.* 2003 Oct 29;30(20):HLS 3-1.
- 769 59. Fraser RH, Olthof I, Carri re M, Deschamps A, Pouliot D. Detecting long-term changes
770 to vegetation in northern Canada using the Landsat satellite image archive. *Environ*
771 *Res Lett.* 2011 Oct 1;6(4):045502.
- 772 60. Ju J, Masek JG. The vegetation greenness trend in Canada and US Alaska from
773 1984–2012 Landsat data. *Remote Sens Environ.* 2016 Apr;176:1–16.
- 774 61. Reynolds MK, Walker DA, Verbyla D, Munger CA. Patterns of Change within a Tundra
775 Landscape: 22-year Landsat NDVI Trends in an Area of the Northern Foothills of the
776 Brooks Range, Alaska. *Arct Antarct Alp Res.* 2013 May 1;45(2):249–60.
- 777 62. Miles VV, Esau I. Spatial heterogeneity of greening and browning between and within
778 bioclimatic zones in northern West Siberia. *Environ Res Lett.* 2016;11(11):115002.
- 779 63. Lara MJ, Nitze I, Grosse G, Martin P, McGuire AD. Reduced arctic tundra productivity
780 linked with landform and climate change interactions. *Sci Rep.* 2018 Feb 5;8(1):2345.
- 781 64. Thompson JA, Koenig LS. Vegetation phenology in Greenland and links to cryospheric
782 change. *Ann Glaciol.* 2018 Dec;59(77):59–68.
- 783 65. Phoenix GK, Bjerke JW. Arctic browning: extreme events and trends reversing arctic
784 greening. *Glob Change Biol.* 2016 Sep 1;22(9):2960–2.
- 785 66. National Academies of Sciences E. Understanding Northern Latitude Vegetation
786 Greening and Browning: Proceedings of a Workshop [Internet]. 2019 [cited 2019 Oct
787 21]. Available from:
788 <https://www.nap.edu/catalog/25423/understanding-northern-latitude-vegetation-greening-and-browning-proceedings-of-a>
- 789
- 790 67. Frost GV, Bhatt US, Epstein HE, Walker DA, Reynolds MK, Berner LT, et al. Arctic
791 Report Card: Update for 2019 - Tundra Greenness [Internet]. Arctic Program. 2019
792 [cited 2019 Feb 23]. Available from:
793 <http://www.arctic.noaa.gov/Report-Card/Report-Card-2015/ArtMID/5037/ArticleID/221/Tundra-Greenness>
- 794
- 795 68. Blok D, Schaepman-Strub G, Bartholomeus H, Heijmans MMPD, Maximov TC,
796 Berendse F. The response of Arctic vegetation to the summer climate: relation between
797 shrub cover, NDVI, surface albedo and temperature. *Environ Res Lett.* 2011 Jul
798 1;6:035502.
- 799 69. Reynolds MK, Walker DA, Epstein HE, Pinzon JE, Tucker CJ. A new estimate of
800 tundra-biome phytomass from trans-Arctic field data and AVHRR NDVI. *Remote Sens*
801 *Lett.* 2012 Sep 1;3(5):403–11.
- 802 70. Berner LT, Jantz P, Tape KD, Goetz SJ. Tundra plant above-ground biomass and shrub
803 dominance mapped across the North Slope of Alaska. *Environ Res Lett.* 2018
804 Feb;13(3):035002.
- 805 71. Cunliffe AM, Assmann JJ, Daskalova G, Kerby JT, Myers-Smith IH. Aboveground
806 biomass corresponds strongly with drone-derived canopy height but weakly with

- 807 greenness (NDVI) in a shrub tundra landscape. *Environ Res Lett* [Internet]. 2020 [cited
808 2020 Jul 10]; Available from: <http://iopscience.iop.org/10.1088/1748-9326/aba470>
- 809 72. Stow D. Remote sensing of vegetation and land-cover change in arctic tundra
810 ecosystems. *Remote Sens Environ*. 2004 Feb;89(3):281–308.
- 811 73. Bartsch A, Widhalm B, Leibman M, Ermokhina K, Kumpula T, Skarin A, et al. Feasibility
812 of tundra vegetation height retrieval from Sentinel-1 and Sentinel-2 data. *Remote Sens*
813 *Environ*. 2020 Feb 1;237:111515.
- 814 74. Woodcock CE, Strahler AH. The factor of scale in remote sensing. *Remote Sens*
815 *Environ*. 1987 Apr 1;21(3):311–32.
- 816 75. Henry GHR, Molau U. Tundra plants and climate change: the International Tundra
817 Experiment (ITEX). *Glob Change Biol*. 1997 Dec 1;3(S1):1–9.
- 818 76. Beck PSA, Jönsson P, Høgda K-A, Karlsen SR, Eklundh L, Skidmore AK. A
819 ground-validated NDVI dataset for monitoring vegetation dynamics and mapping
820 phenology in Fennoscandia and the Kola peninsula. *Int J Remote Sens*. 2007 Oct
821 10;28(19):4311–30.
- 822 77. Gamon JA, Huemmrich KF, Stone RS, Tweedie CE. Spatial and temporal variation in
823 primary productivity (NDVI) of coastal Alaskan tundra: Decreased vegetation growth
824 following earlier snowmelt. *Remote Sens Environ*. 2013 Feb 15;129:144–53.
- 825 78. Kerby JT. Phenology in a changing Arctic: Linking trophic interactions across scales.
826 2015 Sep 14 [cited 2018 Oct 19]; Available from:
827 <https://etda.libraries.psu.edu/catalog/26992>
- 828 79. Anderson K, Gaston KJ. Lightweight unmanned aerial vehicles will revolutionize spatial
829 ecology. *Front Ecol Environ*. 2013 Mar 18;11(3):138–46.
- 830 80. Klosterman S, Richardson AD. Observing Spring and Fall Phenology in a Deciduous
831 Forest with Aerial Drone Imagery. *Sensors*. 2017 Dec;17(12):2852.
- 832 81. Assmann JJ, Kerby JT, Cunliffe AM, Myers-Smith IH. Vegetation monitoring using
833 multispectral sensors — best practices and lessons learned from high latitudes. *J*
834 *Unmanned Veh Syst*. 2018 Dec 5;7(1):54–75.
- 835 82. Klosterman S, Hufkens K, Richardson AD. Later springs green-up faster: the relation
836 between onset and completion of green-up in deciduous forests of North America. *Int J*
837 *Biometeorol*. 2018 Sep 1;62(9):1645–55.
- 838 83. Myers-Smith IH, Hik DS. Shrub canopies influence soil temperatures but not nutrient
839 dynamics: An experimental test of tundra snow–shrub interactions. *Ecol Evol*. 2013 Oct
840 1;3(11):3683–700.
- 841 84. Smith C, Kennedy C, Hargrave A, McKenna K. Soil and Vegetation of Herschel Island.
842 Whitehorse, Yukon Territory, Canada: Agriculture Canada; 1989. Report No.: No 1.
- 843 85. Obu J, Lantuit H, Myers-Smith I, Heim B, Wolter J, Fritz M. Effect of Terrain
844 Characteristics on Soil Organic Carbon and Total Nitrogen Stocks in Soils of Herschel
845 Island, Western Canadian Arctic. *Permafrost Periglacial Process*. 2015 Jan 1;28(1):92–107.
- 846 86. Myers-Smith IH, Hik DS, Kennedy C, Cooley D, Johnstone JF, Kenney AJ, et al.
847 Expansion of Canopy-Forming Willows Over the Twentieth Century on Herschel Island,
848 Yukon Territory, Canada. *AMBIO*. 2011 Sep;40(6):610–23.
- 849 87. Raynolds MK, Walker DA, Balser A, Bay C, Campbell M, Cherosov MM, et al. A raster
850 version of the Circumpolar Arctic Vegetation Map (CAVM). *Remote Sens Environ*. 2019
851 Oct 1;232:111297.
- 852 88. Myers-Smith IH, Grabowski MM, Thomas HJD, Angers-Blondin S, Daskalova GN,
853 Bjorkman AD, et al. Eighteen years of ecological monitoring reveals multiple lines of
854 evidence for tundra vegetation change. *Ecol Monogr*. 2019;89(2):e01351.
- 855 89. Didan K. MOD13Q1 MODIS/Terra Vegetation Indices 16-Day L3 Global 250m SIN Grid
856 V006 [Internet]. NASA EOSDIS Land Processes DAAC; 2015 [cited 2018 Oct 22].
857 Available from: <https://doi.org/10.5067/MODIS/MOD13Q1.006>

- 858 90. Gorelick N, Hancher M, Dixon M, Ilyushchenko S, Thau D, Moore R. Google Earth
859 Engine: Planetary-scale geospatial analysis for everyone. *Remote Sens Environ.* 2017
860 Dec 1;202:18–27.
- 861 91. Mueller-Wilm U. Sen2Cor Software Release Note: Ref.:
862 S2-PDGS-MPC-L2A-SRN-V2.4.0 [Internet]. 2017 [cited 2018 Oct 22]. Available from:
863 [http://step.esa.int/thirdparties/sen2cor/2.4.0/Sen2Cor_240_Documentation_PDF/S2-PD](http://step.esa.int/thirdparties/sen2cor/2.4.0/Sen2Cor_240_Documentation_PDF/S2-PDGS-MPC-L2A-SRN-V2.4.0.pdf)
864 [GS-MPC-L2A-SRN-V2.4.0.pdf](http://step.esa.int/thirdparties/sen2cor/2.4.0/Sen2Cor_240_Documentation_PDF/S2-PDGS-MPC-L2A-SRN-V2.4.0.pdf)
- 865 92. Molau U, Mølgaard P. International Tundra Experiment Manual [Internet]. 1996.
866 Available from: <https://www.gvsu.edu/itex/library-8.htm>
- 867 93. Hadfield JD. MCMC Methods for Multi-Response Generalized Linear Mixed Models:
868 The **MCMCglmm** R Package. *J Stat Softw* [Internet]. 2010 [cited 2018 Mar 16];33(2).
869 Available from: <http://www.jstatsoft.org/v33/i02/>
- 870 94. Hijmans RJ. raster: Geographic Data Analysis and Modeling [Internet]. 2020. Available
871 from: <https://CRAN.R-project.org/package=raster>
- 872 95. Pebesma EJ. Multivariable geostatistics in S: the gstat package. *Comput Geosci.*
873 2004;30:683–91.
- 874 96. Gräler B, Pebesma E, Heuvelink G. Spatio-Temporal Interpolation using gstat. *R J.*
875 2016;8(1):204–18.
- 876 97. Fernández-Guisuraga JM, Sanz-Ablanedo E, Suárez-Seoane S, Calvo L. Using
877 Unmanned Aerial Vehicles in Postfire Vegetation Survey Campaigns through Large and
878 Heterogeneous Areas: Opportunities and Challenges. *Sensors.* 2018 Feb;18(2):586.
- 879 98. Fawcett D, Panigada C, Tagliabue G, Boschetti M, Celesti M, Evdokimov A, et al.
880 Multi-Scale Evaluation of Drone-Based Multispectral Surface Reflectance and
881 Vegetation Indices in Operational Conditions. *Remote Sens.* 2020 Jan;12(3):514.
- 882 99. Matese A, Toscano P, Di Gennaro SF, Genesio L, Vaccari FP, Primicerio J, et al.
883 Intercomparison of UAV, Aircraft and Satellite Remote Sensing Platforms for Precision
884 Viticulture. *Remote Sens.* 2015 Mar;7(3):2971–90.
- 885 100. Franzini M, Ronchetti G, Sona G, Casella V. Geometric and Radiometric Consistency
886 of Parrot Sequoia Multispectral Imagery for Precision Agriculture Applications. *Appl Sci.*
887 2019 Jan;9(24):5314.
- 888 101. Khaliq A, Comba L, Biglia A, Ricauda Aimonino D, Chiaberge M, Gay P. Comparison of
889 Satellite and UAV-Based Multispectral Imagery for Vineyard Variability Assessment.
890 *Remote Sens.* 2019 Jan;11(4):436.
- 891 102. Riihimäki H, Luoto M, Heiskanen J. Estimating fractional cover of tundra vegetation at
892 multiple scales using unmanned aerial systems and optical satellite data. *Remote Sens*
893 *Environ.* 2019 Apr 1;224:119–32.
- 894 103. Mark AF, Fetcher N, Shaver GR, III FSC. Estimated Ages of Mature Tussocks of
895 *Eriophorum vaginatum* along a Latitudinal Gradient in Central Alaska, U.S.A. *Arct Alp*
896 *Res.* 1985 Feb 1;17(1):1–5.
- 897 104. Fritz M, Wolter J, Rudaya N, Palagushkina O, Nazarova L, Obu J, et al. Holocene
898 ice-wedge polygon development in northern Yukon permafrost peatlands (Canada).
899 *Quat Sci Rev.* 2016 Sep 1;147:279–97.
- 900 105. Billings WD, Bliss LC. An Alpine Snowbank Environment and Its Effects on Vegetation,
901 Plant Development, and Productivity. *Ecology.* 1959;40(3):388–97.
- 902 106. Suvanto S, Roux PCL, Luoto M. Arctic–alpine vegetation biomass is driven by
903 fine–scale abiotic heterogeneity. *Geogr Ann Ser Phys Geogr.* 2014 Dec
904 1;96(4):549–60.
- 905 107. Riihimäki H, Heiskanen J, Luoto M. The effect of topography on arctic-alpine
906 aboveground biomass and NDVI patterns. *Int J Appl Earth Obs Geoinformation.* 2017
907 Apr;56:44–53.
- 908 108. Stoy PC, Williams M, Spadavecchia L, Bell RA, Prieto-Blanco A, Evans JG, et al. Using

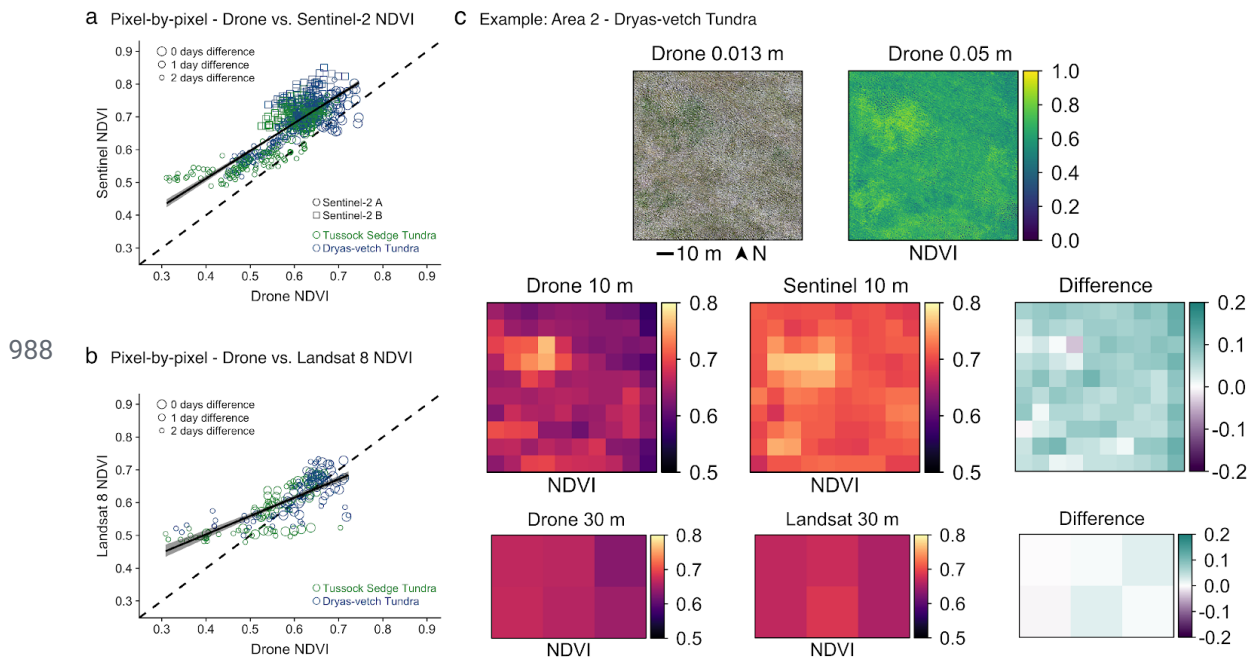
- 909 Information Theory to Determine Optimum Pixel Size and Shape for Ecological Studies:
910 Aggregating Land Surface Characteristics in Arctic Ecosystems. *Ecosystems*. 2009 Jun
911 1;12(4):574–89.
- 912 109. Virtanen T, Ek M. The fragmented nature of tundra landscape. *Int J Appl Earth Obs*
913 *Geoinformation*. 2014 Apr 1;27:4–12.
- 914 110. Høye TT, Post E, Schmidt NM, Trøjelsgaard K, Forchhammer MC. Shorter flowering
915 seasons and declining abundance of flower visitors in a warmer Arctic. *Nat Clim*
916 *Change*. 2013 Aug;3(8):759–63.
- 917 111. Armstrong JB, Takimoto G, Schindler DE, Hayes MM, Kauffman MJ. Resource waves:
918 phenological diversity enhances foraging opportunities for mobile consumers. *Ecology*.
919 2016;97(5):1099–112.
- 920 112. Miller CE, Griffith PC, Goetz SJ, Hoy EE, Pinto N, McCubbin IB, et al. An overview of
921 ABoVE airborne campaign data acquisitions and science opportunities. *Environ Res*
922 *Lett*. 2019 Jul;14(8):080201.
- 923 113. Klosterman S, Melaas E, Wang JA, Martinez A, Frederick S, O’Keefe J, et al.
924 Fine-scale perspectives on landscape phenology from unmanned aerial vehicle (UAV)
925 photography. *Agric For Meteorol*. 2018 Jan 15;248:397–407.
- 926 114. Berra EF, Gaulton R, Barr S. Assessing spring phenology of a temperate woodland: A
927 multiscale comparison of ground, unmanned aerial vehicle and Landsat satellite
928 observations. *Remote Sens Environ*. 2019 Mar 15;223:229–42.
- 929 115. D’Odorico P, Besik A, Wong CYS, Isabel N, Ensminger I. High-throughput drone-based
930 remote sensing reliably tracks phenology in thousands of conifer seedlings. *New*
931 *Phytol*. 2020;226(6):1667–81.
- 932 116. Prevéy J, Vellend M, Rüger N, Hollister RD, Bjorkman AD, Myers–Smith IH, et al.
933 Greater temperature sensitivity of plant phenology at colder sites: implications for
934 convergence across northern latitudes. *Glob Change Biol*. 2017;23(7):2660–71.
- 935 117. Fawcett D, Anderson K. Investigating impacts of calibration methodology and
936 irradiance variations on lightweight drone-based sensor derived surface reflectance
937 products. In: *Remote Sensing for Agriculture, Ecosystems, and Hydrology XXI*
938 [Internet]. International Society for Optics and Photonics; 2019 [cited 2020 Jul 11]. p.
939 111490D. Available from:
940 <https://www.spiedigitallibrary.org/conference-proceedings-of-spie/11149/111490D/Investigating-impacts-of-calibration-methodology-and-irradiance-variations-on-lightweight/10.1117/12.2533106.short>
- 943 118. Huang S, Tang L, Hupy JP, Wang Y, Shao G. A commentary review on the use of
944 normalized difference vegetation index (NDVI) in the era of popular remote sensing. *J*
945 *For Res* [Internet]. 2020 May 31 [cited 2020 Jul 11]; Available from:
946 <https://doi.org/10.1007/s11676-020-01155-1>
- 947 119. Zhang Q, Yao T, Huemrich KF, Middleton EM, Lyapustin A, Wang Y. Evaluating
948 impacts of snow, surface water, soil and vegetation on empirical vegetation and snow
949 indices for the Utqiagvik tundra ecosystem in Alaska with the LVS3 model. *Remote*
950 *Sens Environ*. 2020 Apr 1;240:111677.
- 951 120. Aasen H, Honkavaara E, Lucieer A, Zarco-Tejada PJ. Quantitative Remote Sensing at
952 Ultra-High Resolution with UAV Spectroscopy: A Review of Sensor Technology,
953 Measurement Procedures, and Data Correction Workflows. *Remote Sens*. 2018
954 Jul;10(7):1091.
- 955 121. Strahler AH, Woodcock CE, Smith JA. On the nature of models in remote sensing.
956 *Remote Sens Environ*. 1986 Oct 1;20(2):121–39.
- 957 122. Chen JM. Spatial Scaling of a Remotely Sensed Surface Parameter by Contexture.
958 *Remote Sens Environ*. 1999 Jul 1;69(1):30–42.
- 959 123. Chen JM, Chen X, Ju W. Effects of vegetation heterogeneity and surface topography

- 960 on spatial scaling of net primary productivity. *Biogeosciences*. 2013 Jul
961 18;10(7):4879–96.
- 962 124. Garrigues S, Allard D, Baret F, Weiss M. Influence of landscape spatial heterogeneity
963 on the non-linear estimation of leaf area index from moderate spatial resolution remote
964 sensing data. *Remote Sens Environ*. 2006 Dec 30;105(4):286–98.
- 965 125. Becker RA, Wilks AR, Brownrigg R, Minka TP, Deckmyn A. maps: Draw Geographical
966 Maps [Internet]. 2018. Available from: <https://CRAN.R-project.org/package=maps>
- 967 126. Becker RA, Wilks AR, Brownrigg R. mapdata: Extra Map Databases [Internet]. 2018.
968 Available from: <https://CRAN.R-project.org/package=mapdata>
969

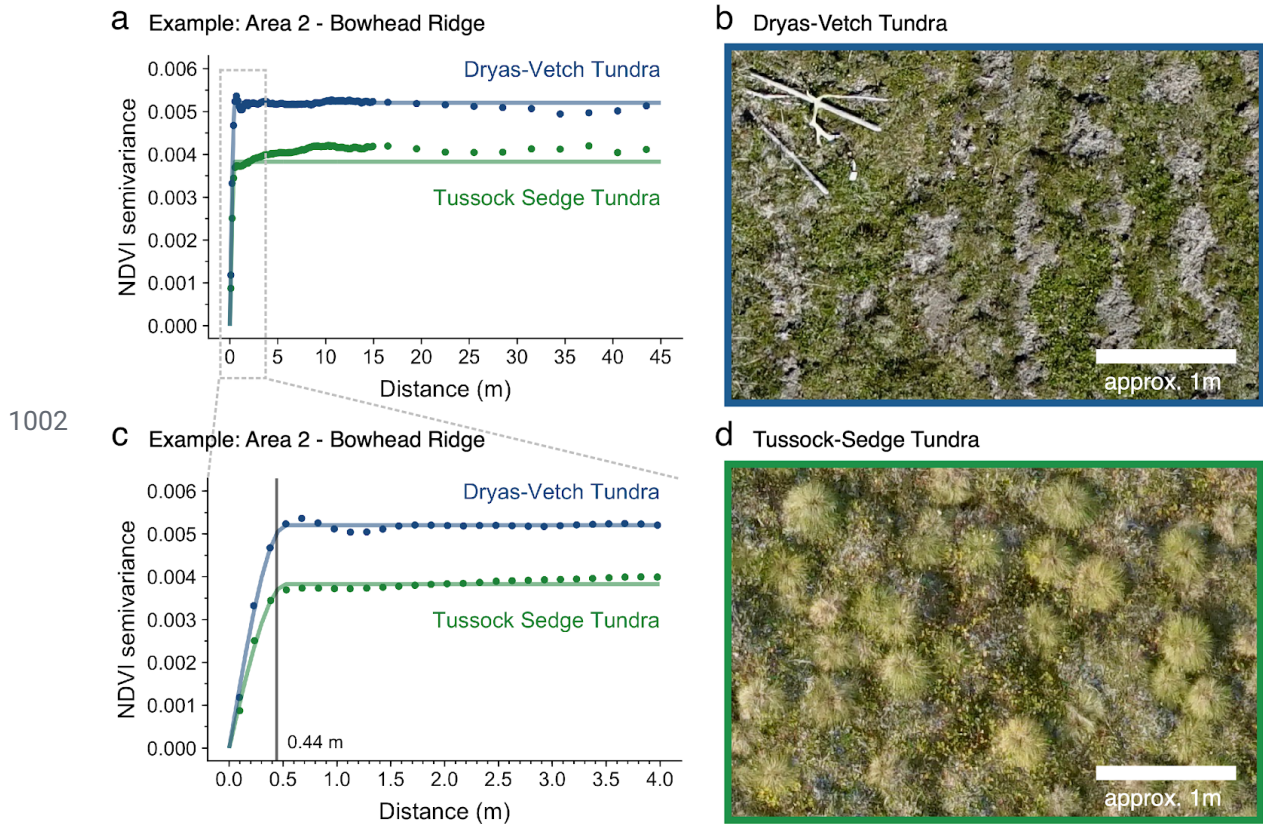


971 **Figure 1:** Drone-data captured the temporal variation in satellite data across vegetation communities, areas and
 972 years. This figure showcases variation in mean landscape greenness (NDVI) across the eight one-hectare
 973 sampling plots on Qikiqtaruk as derived from drone orthomosaics and the MODIS Vegetation Index
 974 (MOD13Q1.v006 Terra), Landsat 8 Level 2 and Sentinel-2 Level-2A products. Vertical dotted grey lines represent
 975 the average snow-melt at long-term monitoring plots close to Area 3 - Hawk Valley for the given year (88).
 976 Dashed grey lines represent simple quadratic phenology curves ($NDVI \sim a x^2 + b x + c$, where x is the day of
 977 year, a the quadratic coefficient, b the linear coefficient and c the y-axis intercept) fitted to all data points pooled
 978 across sensors. The lower central panel demonstrates the close correspondence between seven-day mean
 979 values from drone and satellite NDVI, albeit with a positive offset for all satellite sensors. For this panel, drone
 980 NDVI values were spatially aggregated by mean to the one-hectare plots and temporally aggregated by mean in
 981 consecutive seven-day blocks starting on the first of May in both growing seasons (2016 and 2017) where data
 982 was available. Matching seven-day block pairs between drone and satellite platforms were then identified and
 983 plotted as shown. Spearman's rank correlation as well as mean differences (offsets) in NDVI amongst all platform
 984 combinations can be found in Tables S12 and S13 respectively. The grey dashed line in this panel represents the

985 one-to-one line. Map sources: North America (125,126) in latitude and longitude on the WGS84 reference
986 ellipsoid and Qikiqtaruk, Copernicus Sentinel-2 true colour image July 2017 in UTM 7N based on the WGS84
987 reference ellipsoid.

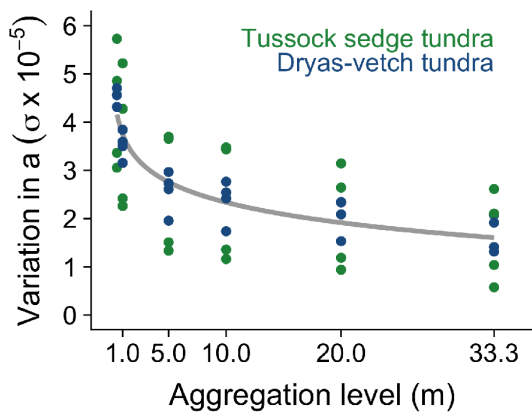


989 **Figure 2:** Drone-data better captured spatial heterogeneity in NDVI relative to Sentinel-2 MSI and Landsat 8 OLI
 990 in pixel-by-pixel comparisons. a) Pixel-by-pixel correlations between 10 m aggregated drone NDVI and native 10
 991 m Sentinel-2 NDVI for a random sample of pixels (10% of total pixels, $n = 700$) across all drone-sentinel image
 992 pairs for the 2017 growing season that were a maximum of two days apart. No drone-sentinel image pairs were
 993 available for the 2016 season that fitted the latter criterium. The black line represents a simple linear model
 994 describing the relationship, see Table S8 for details. b) Pixel-by-pixel correlations between 30 m aggregated
 995 drone NDVI and native 30 m Landsat NDVI for the total number of available pixels ($n = 198$) across all
 996 drone-sentinel image pairs for the 2016 and 2017 growing season. The black line represents a simple linear
 997 model describing the relationship, see Table S10 for details. c) Example visualisations from the Dryas-vetch
 998 tundra at Area 2 - Bowhead Ridge for the 17 July 2017 showing ultra-fine-grain 0.013 m true colour RGB
 999 imagery, 0.05 m native-scale drone NDVI, 10 m resampled drone NDVI, 10 m native Sentinel-2 NDVI, the
 1000 absolute difference between resampled drone and Sentinel-2 NDVI, 30 m resampled drone NDVI, 30 m native
 1001 Landsat 8 NDVI and difference between resampled drone and Landsat 8 NDVI.

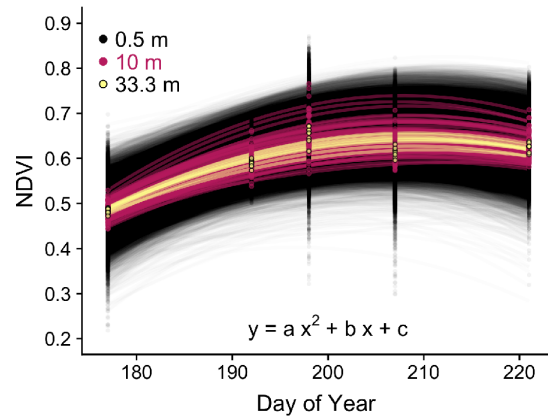


1003 **Figure 3:** Spatial variation of vegetation greenness peaked at distances of ~0.5 m in both studied vegetation
 1004 types, with little or no increase in the spatial dependence of greenness at distances above ~0.5 m. Figure shows
 1005 example variograms. Overall spatial variation in greenness is higher in the Dryas-Vetch Tundra when compared
 1006 to the Tussock-Sedge Tundra (a and c). Left panels: variograms for the Dryas-vetch and tussock sedge tundra
 1007 plots in Area 2 for distances up to 5 m (a) and 45 m (c) at peak season in 2017. The light grey dotted lines in
 1008 panel (a) indicate the subset of the distance range depicted in panel (c). The dark grey line in (c) indicates the
 1009 mean range estimated from the variogram models of both vegetation types from Areas 1, 2, and 4 during
 1010 peak-season (26 and 28 July) in 2017 (see also Figure S1). Right panels: Dryas-vetch tundra with bare ground
 1011 patches caused by cryoturbation and solifluction (c) and tussocks sedge tundra with distinctive patterns of
 1012 tussocks interspersed by patches of willows and herbs (d).

a Variation in quadratic coef. with agg. level

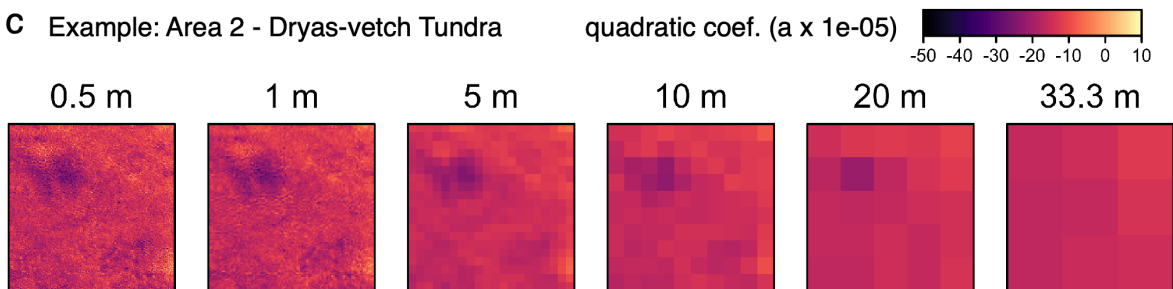


b Example curves: Area 2 - Dryas-vetch Tundra



1013

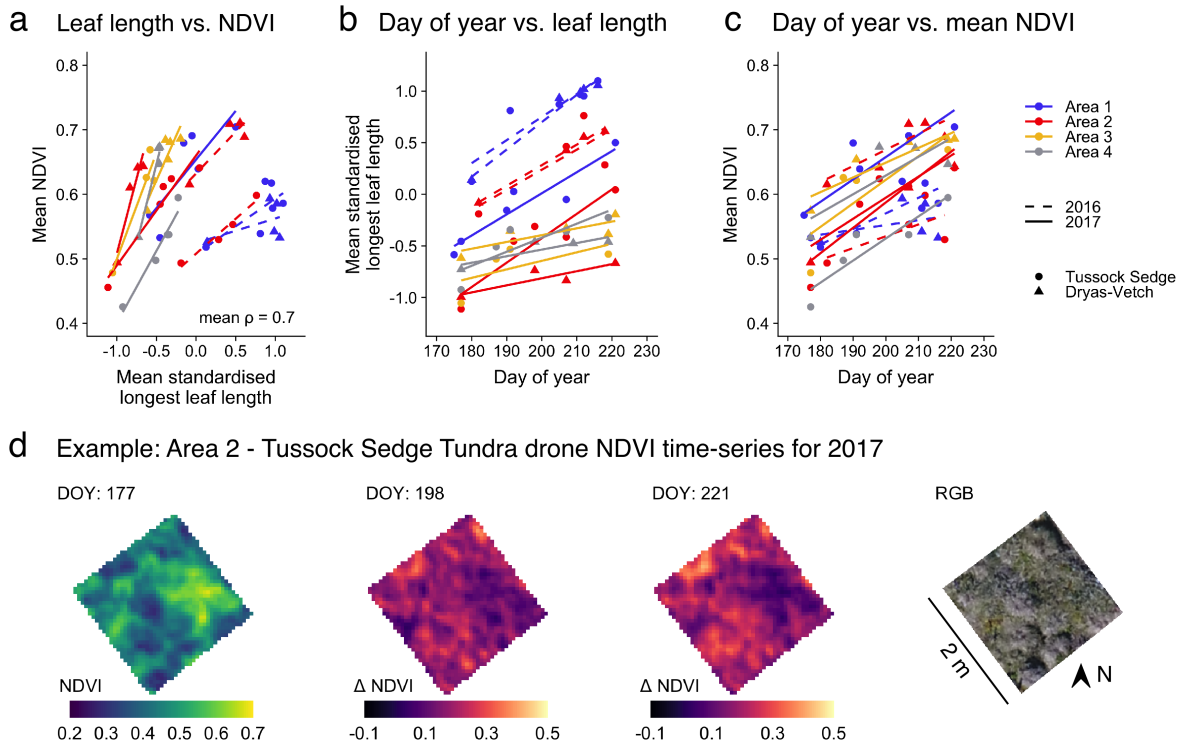
c Example: Area 2 - Dryas-vetch Tundra



1014 **Figure 4:** Fine-scale variation representing key ecological heterogeneity in tundra phenology was lost when
 1015 aggregating from ultra-fine-grain drone to medium-grain satellite pixel sizes. We observed a logarithmic decay in
 1016 variation (standard deviation) in the quadratic coefficient of simple growing season curves fitted to the eight
 1017 vegetation plots in the 2017 season when aggregating the drone data across grain sizes (a). To provide an
 1018 example of the underlying raw data, we visualised the pixel-by-pixel curves fitted to the time-series of pixels from
 1019 the dryas-vetch tundra plot in Area 2 for a subset of three grain sizes (b). Here, each point represents a pixel
 1020 NDVI value at a given day of year and grain size (indicated by colour). The transparent lines represent the simple
 1021 quadratic curves fitted to each pixel across the time-series, again the colour of the line indicates the pixel's
 1022 associated grain-size. See also Figure S8, which shows a random sample of nine curves for all grain sizes from
 1023 the same study plot. Furthermore, to provide an example of the spatial distribution of the quadratic coefficient and
 1024 how it changes across grain sizes, we plotted the respective rasters for Area 2 dryas-vetch tundra in panel (c).
 1025 Similar patterns are found across all areas (a).

1026

1027



1028 **Figure 5:** Time-series of ground-based plot mean standardised longest leaf lengths correlated well with
 1029 drone-derived mean NDVI on Qikiqtaruk. a) Correlations between the mean standardised longest leaf length for
 1030 all individuals across all monitored species and the drone-derived NDVI in the 2 m x 2 m ground-phenology plot
 1031 for each area, vegetation types and year combination. The time-series of mean standardised longest leaf length
 1032 (b) and drone NDVI (c) corresponding to the values in (a). Lines represent least-square regressions to illustrate
 1033 the relationships for each area, vegetation type and year combination. A species-by-species version using
 1034 absolute mean longest leaf length for each plot can be found in Figure S7. (d) As an example, we illustrate the
 1035 drone-based NDVI observations by showing the start, midpoint and end of the timeseries for the 2 m x 2 m
 1036 ground-validation plot in the tussock sedge tundra of Area 2 in 2017. The first time-point in (c) represents the
 1037 greenness in the plot at the beginning of the time-series, the two subsequent plots show the relative difference in
 1038 greenness to this first observation at the given day of year (DOY), and the final plot shows a true-colour image of
 1039 the plot taken by drone on the 17 July 2017 (DOY 198).